Roche E.T., Fabozzo A., Lee Y., Polygerinos P., Friehs I., Schuster L., Whyte W., Casar Berazaluce A.M., Bueno A., Lang N., Pereira M.J.N., Feins E., Wasserman S., O'Cearbhaill E.D., Vasilyev N.V., Mooney D.J., Karp J.M., del Nido P.J., Walsh C.J. "A Light-Reflecting Balloon Catheter for Atraumatic Tissue Defect Repair." *Science Translational Medicine*. September 2015; 7(306):306ra149.

http://stm.sciencemag.org/content/7/306/306ra149.abstract

Science Translational Medicine
AAAS

A Light-Reflecting Balloon Catheter for Atraumatic Tissue Defect Repair

Ellen T Roche[1,2]†, Assunta Fabozzo[3,4]†, Yuhan Lee[5]‡, Panagiotis Polygerinos[1,2]‡, Ingeborg Friehs[3]‡, Lucia Schuster[1,2,7], William Whyte[1,2], Alejandra Maria Casar Berazaluce[3], Alejandra Bueno[3], Nora Lang[3], Maria J.N. Pereira[5,6], Eric Feins[3], Steven Wasserman[8], Eoin D. O'Cearbhaill[5,9], Nikolay V. Vasilyev[3], David J. Mooney[1,2], Jeffrey M. Karp[5], Pedro J. del Nido[3*], Conor J. Walsh[1,2*]

[1]School of Engineering and Applied Science, Harvard University, 29 Oxford Street, Cambridge, MA 02138

[2]Wyss Institute for Biologically Inspired Engineering at Harvard, 3 Blackfan Circle, Boston, MA 02115, USA

[3]Department of Cardiac Surgery, Boston Children's Hospital, Harvard Medical School, 300 Longwood Avenue, Boston, MA 02115, USA

[4]Department of Pediatric Cardiac Surgery, Alma Mater Studiorum, University of Bologna, Via Massarenti 9, 40126 Bologna, Italy.

[5]Division of Biomedical Engineering, Department of Medicine, Center for Regenerative Therapeutics, Brigham and Women's Hospital, Harvard Medical School, Harvard Stem Cell Institute, Harvard-MIT Division of Health Sciences and Technology, 65 Landsdowne Street, Cambridge, MA 02139, USA.

[6]Gecko Biomedical, 74 rue du Fabourg, Saint Antoine 75012, Paris, France

[7]Department of Mechanical Engineering, Technical University of Munich, Boltzmannstrasse 15, 85748 Garching n. Munich, Germany

[8]Department of Biological Engineering, Massachusetts Institute of Technology, 500 Main Street, Cambridge, MA 02139, USA

[9]School of Mechanical and Materials Engineering, University College Dublin, Belfield, Dublin 4, Ireland

*Correspondence to: walsh@seas.harvard.edu (C.J.W); pedro.delnido@cardio.chboston.org (P.J.d.N.)

† These authors contributed equally and are first co-authors

‡ These authors contributed equally and are second co-authors

One Sentence Summary: We present a catheter-based technology that reflects ultra-violet light to activate a photo-curable adhesive for minimally invasive, atraumatic tissue defect closure.

Abstract: A congenital or iatrogenic tissue defect often requires closure by open surgery or metallic components that can erode tissue. Biodegradable, hydrophobic light-activated adhesives represent an attractive alternative to sutures, but lack a specifically designed minimally invasive delivery tool, which limits their clinical translation. We developed a multi-functional, catheter–based technology with no implantable rigid components that functions by unfolding an adhesive-loaded elastic patch and deploying a double-balloon to stabilize and apply pressure to the patch against the tissue defect site. The device uses a fiber optic system and reflective metallic coating to uniformly disperse ultraviolet light for adhesive activation. Using this device, we demonstrate closure on the distal side of a defect in porcine abdominal wall, stomach and heart tissue *ex vivo* . The catheter was further evaluated as a potential tool for tissue closure *in vivo* in a small animal and as a perventricular tool for closure of a challenging cardiac septal defect in a large animal model. Patches attached to the heart and abdominal wall with the device showed similar inflammatory response as sutures, with 100% small animal survival, indicating safety. In the large animal model, a ventricular septal defect in a beating heart was reduced from to <2mm. This new therapeutic platform has utility in a range of clinical scenarios that warrant minimally invasive and atraumatic repair of hard-to-reach defects.

Introduction

Congenital, acquired or iatrogenic defects in visceral organs warrant rapid and effective closure. Internal heart, abdominal, and intestinal defects are challenging to repair. Open surgery has been the standard approach, but minimally invasive (endoscopic and catheter-based) diagnosis and therapy offer a potentially safer alternative with less surgical time and faster recovery periods. Intracardiac septal defects are the most common congenital defects in the young *(1)*. The gold standard treatment is suture-based surgical closure, requiring cardiopulmonary bypass, which can increase to the risk of pump-related complications (for example brain injury from inadequate cerebral perfusion) *(2, 3)*. Multiple transcatheter metallic occluder devices exist *(4, 5)*, but have inherent limitations of cardiac erosion, conduction system block and thrombus formation owing to their bulky and permanent nature *(6–8)*.

For abdominal hernias, wall reinforcement can be achieved surgically or laparoscopically by attaching a mesh patch to the wall using tacks or sutures *(9–12)*. These structures can lead to further complications or hernia recurrence *(13)*. Innovation in mesh fixation and a laparoscopic device that uses an elastomeric adhesive would be desirable and could be rapidly translated to

the clinic. Another clinical example of a tissue defect, a peptic ulcer, can perforate and result in a hole in the bowel wall if not treated properly and promptly. The hole can be medically managed or treated surgically or laparoscopically *(14–16)*. Initial results from a "natural orifice transluminal endoscopic surgery" (NOTES) device are promising for quick recovery times, but these approaches leave permanent clips in the body *(17)*. A similar approach to NOTES that does not leave permanent materials behind, but rather a scaffold that facilitates native tissue healing, could be advantageous for clinical translation.

Lang *et al.* recently demonstrated the feasibility to adhere an elastic biodegradable patch and hydrophobic, light-activated adhesive to an intact septum for quick and effective, atraumatic defect closure in heart tissue and vessels. They showed successful attachment and similar cardiac output compared to a suture-based patch attachment at three months in a small animal model *(18)*. Such a biodegradable occluder could act as a temporary scaffold to facilitate the ingrowth of fibrous connective tissue and endothelialization while the patch and glue are gradually absorbed and replaced by native tissue. Advancing clinical translation of this approach requires the engineering of minimally invasive tools to deliver the adhesives with optional accompanying materials for closure reinforcement. Here, we describe a defect closure device that can affix an elastomeric patch on a blind site via a minimally invasive delivery approach using a photocurable adhesive. Our catheter device enables delivery of a patch coated with a photocurable adhesive, unfolds the patch, reflects and spreads ultra-violet (UV) light from an internal optical fiber, and applies pressure from each side of the wall to stabilize and activate the adhesive on the distal side of the defect. We demonstrate proof-of-concept in three representative examples of the closure of the described congenital or acquired defects: intracardiac defects, abdominal wall hernias and perforated peptic ulcers. This list is by no means exhaustive and can potentially be extended to defect closure of any hollow visceral organ defects (for example perforations in the bowel, bladder, and esophagus).

Results:

A transcatheter light-reflecting technology that delivers and activates a photocurable adhesive

The concept and envisioned clinical applications for the catheter-based closure device are depicted in Fig. 1A, for application in intracardiac defect closure, abdominal hernia repair, and peptic ulcer closure. In brief, the concept of the catheter-based device is that UV light is delivered via an internal fiber optic to a reflective balloon where it is reflected onto a patch pre-coated with photocurable adhesive (Fig. 1B) to affix the patch to the tissue, prior to removal of the device. The functional components of the device included a reflective distal balloon fixed on an inner shaft and a proximal stabilizing balloon on an intermediate shaft (Fig. 1C). All components could be loaded into an outer shaft. A UV fiber optic (connected to a UV source at one end, and designed for light dispersion at the other) was housed in the inner shaft, and could be advanced into the inner lumen until the tip was located in the distal balloon. The reflective distal balloon has an outer layer that allowed temporary suture-based attachment of a patch/adhesive system (Fig. 1C), ensuring the patch unfolds with the balloon and can be released from the system *in situ*.

All components could be deflated and loaded into the outer catheter shaft for delivery (Fig. 1D). The procedural steps are as follows [and depicted in Fig. 1E (side view), Fig. 1F (view from distal side), and movie S1]: i) the catheter is delivered through the defect, ii) the patch is released by pulling back the open suture loop connecting the patch to an outer membrane on the reflective balloon, iii) balloons are deployed (distal balloon first, then proximal), iv) UV light is turned on to activate the photocurable adhesive coated on the proximal side of the patch, and v)

both balloons are fully deflated and removed from the body. In the last step, the distal reflective balloon is retrieved through a four-leaflet valve in the patch, leaving the patch adhered to the tissue. Each shaft can be connected to an ergonomic handle, which allows coupling and uncoupling of shafts, and enables volume-controlled inflation and deflation of the balloons via a syringe (fig. S1 to S5).

Development and optimization of a light-reflective, flexible medical balloon

A metallic coating process for existing urethane medical balloons was developed to reflect light from an internal fiber optic to activate a photocurable adhesive.

To select the optimal reflective coating, a reflectance test was performed on urethane samples coated with various metallic coatings deposited on urethane specimens on silicon wafers, then transferring them to glass slides and mounting them in a test set-up (Fig. 2A) to allow comparison of reflectance between samples. A mirror with >99% reflectivity was used as a positive control. Plasma pre-treatment, which enhances adherence of metallic coating to urethane substrate, improved reflectivity of both aluminum and palladium (Fig. 2B, table S1). To select an outer protective coating to prevent aluminum/blood contact, urethane, gold, and parylene were coated on aluminum samples and the reflectivity test was repeated. All outer coatings resulted in similar reflectivity (Fig. 2C, table S2).

Aluminum particles were deposited on the balloons when a direct current was applied under vacuum (4 mtorr) (Fig. 2D). Urethane balloons were masked on their flat face and taped onto a rotating mount in a sputter chamber (Fig. 2E). Figure 2F shows resulting balloons with a coating of 100 nm of aluminum. The final multi-step coating process is shown in Fig. 2G. A urethane balloon was pre-treated with plasma, coated with 100 nm of aluminum, and a second outer urethane balloon was applied to act as a barrier between the coating and the external environment and to participate in the patch deployment/release mechanism. The coating

thickness varied slightly, but predictably, with distance from aluminum source (fig. S6). The adhesion of the coating was improved with parylene pre-treatment (fig. S7).

Optimization of a low-profile fiber optic cable for light dispersion

To disperse the reflected light on to a relatively large area, the internal fiber optic cable delivering the light was sculpted. By shaping the tip of the internal fiber optic and moving it relative to the reflective chamber (varying the insertion distance), reflected light rays are spread over a larger area compared to a flat tip. Light ray trace simulations were used to examine the effect of the fiber tip angle (straight and 20º conical tip) and the fiber depth (0, 10, and 18.5 mm from the flat face of the balloon) for a given inflated balloon geometry (Fig. 3A, B; fig. S8 and S9; movie S2). The resulting light irradiance maps demonstrate that a sculpted conical fiber results in more spreading of the light on the adhesive/patch system compared to a flat fiber tip (Fig. 3B). The favorable spreading of light is emphasized in Fig. 3C and table S3, where light reflectance at each fiber insertion depth was compared. The flat tip had more variability in efficiency, as it is sensitive to fiber position within the inner shaft, the conical tip had greater efficiency, and less sensitivity to position in the shaft (fig. S9).

The final design of the fiber optic was a sculpted conical shape (Fig. 3D), which enabled spreading of light over the entire surface of the 20-mm diameter circular patch by simply moving the fiber along the inner shaft inside the reflective distal balloon. The motion of the fiber acted to 'paint' a uniform irradiance on the patch. Depending on balloon geometry and clinical application, the fiber optic tip can be sculpted in a case-specific manner using such simulations.

Preclinical applications *in vivo* and *ex vivo*

In vivo adhesion force was tested by activating a hydrophobic light-activated adhesive (HLAA) pre-coated on a poly(glycerol sebacate urethane) (PGSU) patch on the surface of the

subcutaneous tissue of a rodent (Sprague Dawley rats, 200-250 g) model using a miniaturized catheter. Patches attached with the device demonstrated similar adhesion to suture-based PGSU patches, with both groups increasing in strength over the course of 2 weeks (Fig. 4A, table S4), likely due to capsule formation around the patch *in vivo*. Adhesion to explanted sections of pig heart, abdominal wall, and stomach was tested by using the light-reflecting device to attach a PGSU patch to a tissue sample with a pre-load of 3 N. Adhesion forces ranged from 0.598-2.541 N (Fig. 4B, table S5).

Additionally, a patch was attached to whole excised porcine hearts and to the septum of a heart pressurized to physiologically relevant levels (20 and 120 mmHg in the right and left ventricles, respectively) under echocardiographic guidance (Fig. 4C), with a set-up described previously *(19)*. An abdominal wall reinforcement procedure was performed in a euthanized porcine model carcass to evaluate the spatial interaction between the device and abdominal organs (Fig. 4D), demonstrating there was adequate space in the abdomen for device use. Feasibility of the procedure and patch attachment to the innermost layer of the abdominal wall was successfully demonstrated. The PGSU patch is designed to degrade over time *(20)*, but, for this application, could be exchanged for a synthetic, non-degrading hernia mesh.

The catheter was further evaluated as a potential endoscopic tool for tissue closure during NOTES treatment of lesions of the gastro-intestinal tract (Fig. 4E). The procedure was performed on a porcine stomach, both in a whole deceased animal and on the lab bench. The catheter was inserted through the esophagus and directed toward a defect artificially created on the anterior free wall of the stomach. The patch was firmly attached on the external surface of the stomach. Additional adhesive was applied with a syringe to seal it, and cured directly with the fiber optic; ultimately this could be achieved with application of a second outer patch with a modification of the device (forward-transmitting light device, fig. S10). The stomach was filled

to capacity (>1 liter) to test patch adhesion to tissue under supraphysiological hyper-distension and no leaks were observed in either stomach (Fig. 4E).

Finally, using the same miniaturized device (Fig. 5A), a PGSU patch (200 μm thick, 4 mm in diameter) was implanted in the abdomen and on the heart of a rodent model, and both were found to have a moderate fibrotic/inflammatory response to sutures over the course of 2 weeks (Fig. 5B-D). The patch was also tested in cyclical and shear loading conditions after adhesion to porcine epicardial tissue with the device (Fig. 5, E and F). A cyclical compressive load was applied. The patch/adhesive system did not change its compressive modulus for a minimum of 100 cycles. In parallel shear testing, the force to separate the patch from the tissue was ~100 Pa and has been shown to be adequate to keep the patch fixed on a vascular defectsubjected to flowing blood *in vivo (18)*.

Refinement of device parameters for intracardiac applications

Previous work demonstrated that the HLAA/PGSU system has sufficient adhesive strength to keep the patch attached to the epicardium, septum or a vascular defect *in vivo* (0.5-2 N/cm^2, depending on test conditions), and presented encouraging initial results for intracardiac applications *(18)*. Here, we demonstrate similar pull-off forces on isolated porcine endocardial tissue when the patches are applied with our device (0.7–4.8 N/cm^2) (Fig. 6A, table S6).

The effects of two factors—patch-to-defect diameter ratio and pressure gradient on burst pressure—were then evaluated in an *in vitro* set-up. A 5-mm defect was created on a piece of porcine heart tissue, closed with a PGSU/HLAA patch with direct UV light application, and then fixed on a chamber providing pressure control and measurement capabilities (Fig. 6B). Two cases were investigated; for case 1, the pressure was higher in the chamber, simulating the patch attached to the RV septal wall (lower pressure ventricle); in case 2, the pressure was higher

outside the chamber, simulating patch attachment to the LV septal wall (higher pressure ventricle). Three different patch-to-defect diameter ratios were investigated (2.3, 1.75 and 1.4) to represent a range of patch sizes. The highest burst pressures were achieved on the simulated LV wall (case 2) with the largest patch (Fig. 6B, table S7).

The device was flexible enough to be used with a transatrial or transvascular approach (fig. S11). The typical pull-back force applied to the device by a surgeon was measured to be approximately 2.5 N using a mechanical tensile tester. The pull-off strength of the patch after application with the device was evaluated using different pre-load values (1, 3, and 5 N) with the same level and time of light activation to adhere a patch to *ex vivo* porcine tissue (Fig. S12). Pull-off forces demonstrated relative insensitivity of adhesion force to pre-load in this range (Fig. 6C, Table S8).

Patch-mediated reduction of ventricular septal defect (VSD) in vivo

Device functionality (delivery, patch deployment, patch stabilization, patch release, light activation, patch adhesion and device removal) was demonstrated with a perventricular approach *in vivo* in a porcine heart. A VSD was created by guiding the balloon catheter device through the septum into the LV (Fig. 7A, B) and the procedure was performed in a beating heart with echocardiographic monitoring (Fig. 7C-G). No intraoperative complications, such as excessive bleeding or arrhythmia, were observed in any of the three animals. The PGSU patch was successfully attached to the septum, as confirmed by echocardiography (Fig. 7, F and G; movies S3-S6) and postmortem gross organ evaluation (Fig. 7H). Pull-off testing was not carried out for *in vivo* tissue samples, as ultrasound echo imaging provided functional data that demonstrated that the patch was sufficiently adhered to the septal wall.

In one case, the VSD was created in a two-step procedure (catheter guidance through the removal, then re-entry into the defect with another device). In this case, a reduction of flow

diameter through the defect was observed from a VSD diameter of 5.5 mm (Fig. 7E) to 1.4 mm (Fig. 7F; movie S3). Reduction in defect to a size of ≤1.6 mm with open heart surgery is considered adequate for humans, as residual defects less than 2 mm are reported to spontaneously close within 1 year *(21)*.

Discussion

We have developed a light-reflecting technology for adhesive patch–mediated defect closure in challenging biological tissues. Our catheter-based device can achieve patch-to-tissue adhesion by transmitting, reflecting, and spreading UV light, with no mechanical anchoring and without leaving any permanent foreign materials in the body. The device was designed to allow minimally invasive access to the defect site with subsequent patch deployment, even in hard-to-access tissues and organs, such as the septum of the heart. The presence of a stabilizing balloon ensured adequate compression forces to achieve adhesive activation. Importantly, for interfacing with the clinic, the entire procedure can be visualized and monitored with 2D and 3D ultrasound or endoscopic guidance. Although devices for closure of body defect openings have been previously proposed *(22–25)*, most are mainly metallic, and rely on mechanical or suture-based attachment, which can erode tissue over time *(7)*. With our catheter-based device, an elastic biodegradable adhesive can provide adequate tissue fixation that is amenable to healing and growing tissues; for instance, in the pediatric population. The device remains in the body for less than five minutes and no long-term adverse device-related complications were seen in preliminary *in vivo* testing in rodents (100% survival rate).

We envision one of the great advantages of our device will be for closing intracardiac defects. A device that delivers and secures a biodegradable elastic patch to the ventricular septal wall is desirable because atraumatic fixation to the septum does not rely on mechanical anchorage of the occluder. Attachment to the septal wall on the left ventricular side is favorable

in terms of pressure gradients. Once secured, an elastic patch/adhesive system prevents tissue erosion and electrical conduction damage, Although biodegradable septal occluders have been developed *(26, 27)*, but they too rely on mechanical anchorage, which may eventually erode tissue or cause perforation *(7, 28)*. A biodegradable patch system to close intracardiac defects has been tested in patients *(29)*. Early prototypes relied on endothelialization while a balloon was inflated, resulting in up to 48 hour wait times. More recently, an immediate patch release device has been described with a biodegradable balloon without adhesive *(30)*; but while promising, challenges were observed in achieving sufficient adhesion so as to avoid dislodgment *(31)*. Encouraging results were reported when the device was used in conjunction with a pH-activated surgical polyethylene glycol adhesive but required a 45 minute adhesive activation time and angiography *(32)*. In contrast, we have demonstrated a maximum wait time of two minutes for adhesive activation without the need for angiography, using non-invasive echocardiographic guidance.

For abdominal hernia repair, the weakened area in the muscle wall can be repaired surgically; however surgery is limited to small hernias with healthy surrounding tissues. Alternatively synthetic mesh patches are attached over the weakened area (hernioplasty) *(11)*. Laparoscopic hernioplasty involves mesh patch placement from inside the abdominal wall and attaching the mesh with hernia tacks *(13)*. This leads to smaller incisions and faster recovery time *(10)* but tack placement is still associated with infection and hernia reoccurrence *(9, 12)*. The use of our device for hernia repair with a patch and biodegradable adhesive can exploit advantages of laparoscopy without the limitations of tacks, as demonstrated here in a porcine model.

Ulcer perforations can have up to a 30% 1-year mortality rate, with intervention-related adverse events being a main contributor to this *(17)*. Surgical options include pyloroplasty and gastrojejunal/gastroduodenal resection and reconstruction *(16)*. The role of endoscopic

procedures for treatment of perforated peptic ulcer in elective and emergency situations is controversial, largely due to the lack of device that seals the ulcer *(14, 15, 33)*. A NOTES procedure to close ulcers is desirable as it does not require general anesthesia *(17)* but the lack of a reliable gastric closure method remains a significant barrier to the widespread adoption of such procedures *(34)*. Our initial demonstration of the closure of a hole in the pig stomach highlights the potential for such an approach to address this; in particular, the use of a double patch system (which is possible with our device) may be beneficial to achieving secure closure.

Although this study demonstrates proof of concept using a catheter and innovative biomaterials to securely repair atraumatic tissue defects, we have identified some limitations that will need to be addressed prior to translation. First, for the *in vivo* porcine model experiments, the catheter was inserted through an artificially created defect in the right ventricular wall, but for future clinical applications an endovascular or transatrial approach would be more likely. Although this is possible with the existing forward- transmitting light device as previsouly described this could also be achieved with an even more flexible version of the current device in combination with a guide wire to help to navigate the device to the target site. Second, the catheter-based device is removed through the patch, leaving a minimal residual hole. This small hole may be acceptable for a variety of clinical applications (for example, septal defects) but may not be suitable for others (gastrointestinal defects). Conversely, our forward-transmitting light device does not leave any residual hole.

Having demonstrated the feasibility of this approach for enabling atraumatic repair of tissue defects in a minimally invasive manner, future advances can focus on optimization for use in a clinical setting. Sufficient light transmission could be achieved with a more flexible mechanism through the use of multiple fiber bundles, sculpted to have a conical shape tip. Incorporation of a guide wire lumen that would enable tracking of the device along a pre-placed wire. The residual hole in the patch could be sealed by a catheter that could apply and cure

additional adhesive following retraction through the patch; or, a second catheter could apply a patch on the opposite side of the tissue. Additional work exploiting patch elasticity and valve design would be required to achieve central defect sealing, as demonstrated, for example, in the Permaseal^{TM} apical closure device (Micro Interventional Device, Inc.).

The device presented here has numerous potential applications, and although the experiments here were conducted with PGSU and HLAA any optically transparent patch material (e.g. pericardium, dacron, polyurethane), could be used. The device is scalable, and size or geometry of the balloon or patch can be specified based on patient-specific needs (e.g. from pre-procedural imaging). Further applications include closure of other cardiac defects, such as atrial septal defect, patent foramen ovale, and iatrogenic defects created by transcatheter procedures including transapical and trans-septal valve replacements. Besides perforated peptic ulcers, additional gastrointestinal applications could include duodenal/esophageal ulcer perforations and bowel perforations. Without adhesive, the device could be used for photodynamic therapy, which is FDA-approved for endobronchial and esophageal cancers and is being investigated for ovarian *(35)* and breast cancers as well as tumors of the retina *(36)* or to reflect light for crosslinking of vascular tissue, treatment of varicosity, or delivery of low-power laser for encouraging stem cell-based regeneration *(37)*.

In conclusion, we present a catheter-based device that can occlude body defect openings through deployment of adhesive biodegradable elastic materials. The device can reduce the invasiveness of surgical procedures, reduce operative times, and consequently improve the outcome of these procedures without adverse effects. The catheter-based system has promise to accelerate clinical translation for procedures using photocurable adhesives, elastic and soft materials and entirely biodegradable closure systems that may be especially important for atraumatic closure of delicate and friable tissue.

Materials and Methods:

Study design

The study was designed to prove the concept of a new technology to deliver, transmit and spread UV light to HLAA for minimally invasive defect closure in visceral organs. Testing was unblinded (except for *in vivo* histology, which was blinded) but randomized. For reflectivity testing, a 99% reflective mirror was used as a positive control with a sample size of four. Light simulations were run for three conditions with two fiber designs. A sample size of three was used for burst pressure testing, adhesive force testing on tissue (heart tissue, stomach tissue and abdominal wall tissue specimens), and a sample size of seventeen was used for endocardial vs epicardial adhesion testing. The *in vivo* pull-off testing had a sample size of five. Sample sizes for *ex vivo* proof-of-concept testing were one to three. Finally, proof of concept of device functionality *in vivo* was demonstrated in a large animal model of cardiac septal defect, and repeated for three successful experiments. The endpoint was successful patch attachment. We acknowledge that sample sizes are small due to tissue and animal availability; however, we feel that we have sufficient data to demonstrate the feasibility of the approach.

Demonstration of representative clinical applications *ex vivo* and *in vivo*

In vivo. PGSU patches (200 µm thick, 4 mm in diameter) were attached to subcutaneous tissue (n=5), abdomen (*n*=2) or heart (*n*=2) of Sprague Dawley rats by activating a layer of pre-coated HLAA with a miniaturized device connected to a UV-light source (OmniCure S2000, Lumen Dynamics Group Inc.) for 15 seconds at 100% intensity with a filter in the range of 320 to 390 nm). Patches attached to the abdominal subcutaneous tissue (*n*=5 at 1, 7, and 14 days) were compared to suture based attachment for pull-off force. A micro-gripper was used to grasp the patch at one edge and standard pull-off adhesion testing was performed on an Instron 5566

(100-N load cell). Patches on abdominal subcutaneous tissue and the heart were processed for histology (n=2 at 1, 7, and 14 days) and H&E staining.

Ex vivo. Fresh whole porcine hearts (n=3) were used to demonstrate procedural steps. Steps were performed (i) under direct vision with ventricular walls removed (n=2) or (ii) blindly (n=1). To simulate the pressurized heart, a fresh porcine heart was explanted (Fig. 4C), both the aortic valve leaflets were removed, and the pulmonary artery and aorta were securely connected to saline columns at 20 and 100 mmHg respectively. Echocardiography was used to image the procedure. The procedure was then performed in a porcine carcass to evaluate patch attachment to the innermost layer of the abdominal wall (parietal peritoneum). A midline incision of the abdominal wall was performed to visualize the procedure. A 6-mm incision was made on the skin of the abdomen and a subcutaneous tunnel was created to facilitate device insertion (Fig. 4D). Fresh porcine stomach (n=2) was used for testing procedural feasibility and patch attachment to the outer surface of the stomach. In an animal carcass, an incision of 5 mm was made on the anterior free wall of the stomach to represent a peptic ulcer. The device was inserted through the esophagus, and patch was attached to the outer wall. To represent a distended stomach, a second stomach was explanted and mounted on a hanging support. The patch was adhered with the catheter (Fig. 4E). 1ml of HLAA was added to the valve in the patch from the outside with a syringe and cured directly with the fiber optic from the device to seal. The organ was filled to capacity (>1L).

Pull-off and burst pressure testing

Isolated fresh porcine abdominal wall, stomach, and cardiac tissue (n=3) samples were collected from euthanized pigs. A PGSU patch (200-µm thick, 20 mm in diameter) was attached to the tissue by activating a layer of pre-coated HLAA with the device (120 seconds activation at 3 N pre-load) connected to a UV-light source (OmniCure S2000, Lumen Dynamics Group Inc.), at

100% intensity with a filter in the range of 320 to 390 nm. The tissue samples were kept wet with saline throughout the testing. Standard pull-off adhesion testing was performed on an Instron 5566 (1 kN load cell). Briefly, the adherent PGSU patch was attached to a flat probe using cyanoacrylate glue (Loctite 4601) a compressive preload of 1 N was applied for 5 seconds and the patch was pulled off at a rate of 8 mm/min. For pre-load testing, testing on epicardium was repeated after adhesion with various preloads (1, 3, and 5 N applied with the tensile tester). Further pull-off testing was performed with identical patches and fresh porcine endocardial and epicardial tissue and as previously described *(18)*. Burst pressure testing was performed on porcine myocardium with the HLAA-coated PGSU patch as described in the supplementary methods.

***In vivo* porcine testing**

The animal protocol was reviewed and approved by the Boston Children's Hospital Institutional Animal Care and Use Committee. All animals received humane care in accordance with the Guide for the Care and Use of Laboratory Animals recommended by the US National Institute of Health. Yorkshire female pigs, weighing 40-50 kg were used. Briefly, a right side antero-lateral thoracotomy was performed, in the 4^{th} intercostal space, and the pericardium was opened. Two concentric purse-string sutures (3-0 polypropylene) were placed on the right ventricular wall for the device insertion. Echocardiography was used for imaging. No cardiopulmonary bypass was used. The device was inserted and advanced through the interventricular septum into the LV (to create the VSD), then retracted into the RV and the procedural steps previously described were carried out.

Statistical methods

Datasets are included in the supplementary materials (tables S1-S8). Graphpad Prism software was used for statistical analysis and graphs. For each dataset a histogram was first constructed to assess the distribution of the data, and summary statistics, including the mean and median were calculated. For non-normally distributed data a two-tailed Mann Whitney test was used for pairwise comparisons (with Dunnetts's post-hoc test), and Kruskal-Wallis one-way analysis for multiple comparisons (with Dunn's post-hoc test). Results were considered significant when a P value of ≤ 0.05 was obtained, and alpha level was adjusted for multiple comparisons.

Supplementary Materials:

Materials and Methods
Figure S1: Handle component design.
Figure S2: Decoupling mechanism for handle components.
Figure S3: Engineering drawing of the raster rod.
Figure S4: Engineering drawing of the slider sleeve.
Figure S5: Engineering drawing of the handle body.
Figure S6: Energy dispersive electron spectrometry.
Figure S7: Adhesion testing of the aluminum deposition process on parylene coated urethane samples.
Figure S8: The inflated balloon approximates an axicon for light simulations.
Figure S9: Light ray analysis for flat and conical tipped fibers.
Figure S10: A modified catheter for direct application of light.
Figure S11: Demonstration of transvascular access in the porcine heart.
Figure S12: The patch adheres to the endocardial tissue.
Table S1: Reflectivity with various coatings ± plasma pre-treatment.
Table S2: Reflectivity with various outer coatings.
Table S3: Efficiency for flat and conical tip fiber.
Table S4: Pull-off forces *in vivo* for rat tissues on subcutaneous abdomen.
Table S5: Pull-off forces for *ex vivo* porcine tissues (endocardium, abdominal wall and stomach).
Table S6: Pull-off forces for endocardium and epicardium.
Table S7: Burst pressures for case 1 and case 2 for various patch/defect ratios.
Table S8: Pull-off forces for different pre-loads.
Movie S1: Overview of device functioning.
Movie S2: Light analysis as conical tip is moved into balloon.
Movie S3: Doppler flow before and after VSD closure.
Movie S4: Patch deployment *in vitro* and *in vivo*.
Movie S5: Patch stabilization *in vitro* and *in vivo*.
Movie S6: Adhered patch *in vivo* in beating heart.

Reference (*43*)

References and notes:

1. J. Hoffman, S. Kaplan, The incidence of congenital heart disease, *J AM Coll Cardiol* **39**, 1890–1900 (2002).

2. J. W. Newburger, R. A. Jonas, G. Wernovsky, D. Wypij, P. R. Hickey, K. C. Kuban, D. M. Farrell, G. L. Holmes, S. L. Helmers, J. Constantinou, *A comparison of the perioperative neurologic effects of hypothermic circulatory arrest versus low-flow cardiopulmonary bypass in infant heart surgery.* (1993; http://www.nejm.org/doi/pdf/10.1056/NEJM199310073291501).

3. D. C. Bellinger, R. a Jonas, L. a Rappaport, D. Wypij, G. Wernovsky, K. C. Kuban, P. D. Barnes, G. L. Holmes, P. R. Hickey, R. D. Strand, Developmental and neurologic status of children after heart surgery with hypothermic circulatory arrest or low-flow cardiopulmonary bypass., *N. Engl. J. Med.* **332**, 549–55 (1995).

4. R. Kozlik-Feldmann, N. Lang, R. Aumann, A. Lehner, D. Rassoulian, R. Sodian, C. Schmitz, M. Hinterseer, R. Hinkel, E. Thein, F. Freudenthal, N. V Vasilyev, N. V Vasylev, P. J. del Nido, H. Netz, Patch closure of muscular ventricular septal defects with a new hybrid therapy in a pig model., *J. Am. Coll. Cardiol.* **51**, 1597–603 (2008).

5. P. Ewert, F. Berger, I. Daehnert, J. van Wees, M. Gittermann, H. Abdul-Khaliq, P. E. Lange, Transcatheter Closure of Atrial Septal Defects Without Fluoroscopy : Feasibility of a New Method, *Circulation* **101**, 847–849 (2000).

6. D. Predescu, R. R. Chaturvedi, M. K. Friedberg, L. N. Benson, A. Ozawa, K.-J. Lee, Complete heart block associated with device closure of perimembranous ventricular septal defects., *J. Thorac. Cardiovasc. Surg.* **136**, 1223–8 (2008).

7. G. B. Crawford, R. G. Brindis, M. W. Krucoff, B. P. Mansalis, J. D. Carroll, Percutaneous atrial septal occluder devices and cardiac erosion: a review of the literature., *Catheter. Cardiovasc. Interv.* **80**, 157–67 (2012).

8. U. Krumsdorf, S. Ostermayer, K. Billinger, T. Trepels, E. Zadan, K. Horvath, H. Sievert, Incidence and clinical course of thrombus formation on atrial septal defect and patient foramen ovale closure devices in 1,000 consecutive patients, *J. Am. Coll. Cardiol.* **43**, 302–309 (2004).

9. R. Shalaby, M. Ismail, A. Samaha, A. Yehya, R. Ibrahem, S. Gouda, A. Helal, O. Alsamahy, Laparoscopic inguinal hernia repair; experience with 874 children., *J. Pediatr. Surg.* **49**, 460–4 (2014).

10. L. Neumayer, A. Giobbie-Hurder, O. Jonasson, R. Fitzgibbons, D. Dunlop, J. Gibbs, D. Reda, W. Henderson, Open mesh versus Laparoscopic Mesh Repair of Inguinal Hernia, *N. Engl. J. Med.* **350**, 1819–1827 (2004).

11. J. P. Fischer, J. D. Wink, J. a Nelson, S. J. Kovach, Among 1,706 cases of abdominal wall reconstruction, what factors influence the occurrence of major operative complications?, *Surgery* **155**, 311–9 (2014).

12. S. C. Azoury, A. P. Dhanasopon, X. Hui, C. De La Cruz, S. H. Tuffaha, J. M. Sacks, K. Hirose, T. H. Magnuson, C. Liao, M. Lovins, M. a Schweitzer, H. T. Nguyen, A single institutional comparison of endoscopic and open abdominal component separation., *Surg. Endosc.* (2014), doi:10.1007/s00464-014-3627-2.

13. K. a LeBlanc, Tack hernia: a new entity., *JSLS* **7**, 383–7 (2003).

14. M. H. Møller, S. Adamsen, M. Wøjdemann, A. M. Møller, Perforated peptic ulcer: how to improve outcome?, *Scand. J. Gastroenterol.* **44**, 15–22 (2009).

15. M. J. O. E. Bertleff, J. F. Lange, Laparoscopic correction of perforated peptic ulcer: first choice? A review of literature., *Surg. Endosc.* **24**, 1231–9 (2010).

16. S. Gupta, R. Kaushik, R. Sharma, A. Attri, The management of large perforations of duodenal ulcers., *BMC Surg.* **5**, 15 (2005).

17. J. Bingener, E. a Loomis, C. J. Gostout, M. D. Zielinski, N. S. Buttar, L. M. W. K. Song, T. H. Baron, L. S. Ghahfarokhi, E. Rajan, Feasibility of NOTES omental plug repair of perforated peptic ulcers: results from a clinical pilot trial., *Surg. Endosc.* **27**, 2201–8 (2013).

18. N. Lang, M. J. Pereira, Y. Lee, I. Friehs, N. V Vasilyev, E. N. Feins, K. Ablasser, E. D. O'Cearbhaill, C. Xu, A. Fabozzo, R. Padera, S. Wasserman, F. Freudenthal, L. S. Ferreira, R. Langer, J. M. Karp, P. J. del Nido, A blood-resistant surgical glue for minimally invasive repair of vessels and heart defects., *Sci. Transl. Med.* **6**, 218ra6 (2014).

19. H. Yamauchi, E. N. Feins, N. V Vasilyev, S. Shimada, D. Zurakowski, P. J. Del Nido, Creation of nonischemic functional mitral regurgitation by annular dilatation and nonplanar modification in a chronic in vivo swine model., *Circulation* **128**, S263–70 (2013).

20. M. J. N. Pereira, B. Ouyang, C. a Sundback, N. Lang, I. Friehs, S. Mureli, I. Pomerantseva, J. McFadden, M. C. Mochel, O. Mwizerwa, P. Del Nido, D. Sarkar, P. T. Masiakos, R. Langer, L. S. Ferreira, J. M. Karp, A highly tunable biocompatible and multifunctional biodegradable elastomer., *Adv. Mater.* **25**, 1209–15 (2013).

21. A. Dodge-Khatami, W. Knirsch, M. Tomaske, R. Prêtre, D. Bettex, V. Rousson, U. Bauersfeld, Spontaneous closure of small residual ventricular septal defects after surgical repair., *Ann. Thorac. Surg.* **83**, 902–5 (2007).

22. M. Neuss, F. Freudenthal, US6355052 B1 Device for closure of body defect openings (2002) (available at http://www.google.com/patents/US6355052).

23. D. Balzer, Current Status of Percutaneous Closure of Ventricular Septal Defects, *Pediatr. Ther.* **02** (2012), doi:10.4172/2161-0665.1000112.

24. I. Michel-Behnke, P. Ewert, A. Koch, H. Bertram, M. Emmel, G. Fischer, R. Gitter, R. Kozlik-Feldman, R. Motz, E. Kitzmüller, O. Kretschmar, Device closure of ventricular septal defects by hybrid procedures: a multicenter retrospective study., *Catheter. Cardiovasc. Interv.* **77**, 242–51 (2011).

25. P. Chungsomprasong, K. Durongpisitkul, C. Vijarnsorn, J. Soongswang, T. P. Lê, The results of transcatheter closure of VSD using Amplatzer® device and Nit Occlud® Lê coil., *Catheter. Cardiovasc. Interv.* **78**, 1032–40 (2011).

26. G. Morgan, K.-J. Lee, R. Chaturvedi, L. Benson, A biodegradable device (BioSTAR) for atrial septal defect closure in children., *Catheter. Cardiovasc. Interv.* **76**, 241–5 (2010).

27. Y. Zhu, X. Huang, J. Cao, J. Hu, Y. Bai, H. Jiang, Z. Li, Y. Chen, W. Wang, Y. Qin, X. Zhao, Animal experimental study of the fully biodegradable atrial septal defect (ASD) occluder., *J. Biomed. Biotechnol.* **2012**, 735989 (2012).

28. E. Ivens, C. Hamilton-Craig, C. Aroney, A. Clarke, H. Jalali, D. J. Burstow, Early and late cardiac perforation by Amplatzer atrial septal defect and patent foramen ovale devices., *J. Am. Soc. Echocardiogr.* **22**, 1067–70 (2009).

29. E. B. Sideris, B. Macuil, V. Varvarenko, S. Toumanides, Transcatheter patch occlusion of perimembranous ventricular septal defects., *Am. J. Cardiol.* **95**, 1518–21 (2005).

30. B. Sideris, E. Sideris, M. Calachanis, V. Papantoniou, S. Moulopoulos, The immediate release patch in the correction of experimental atrial septal defects., *Catheter. Cardiovasc. Interv.* **76**, 572–7 (2010).

31. E. M. Rad, P. N. Davari, H. Mortezaeian, Embolization of Immediate Release Transcatheter Patch for Atrial Septal Defect Occlusion: The Causes and the Pitfalls to Avoid, *J. Invasive Cardiol.* **24** (2012).

32. S. Toumanides, E. B. Sideris, T. Agricola, S. Moulopoulos, Transcatheter patch occlusion of the left atrial appendage using surgical adhesives in high-risk patients with atrial fibrillation., *J. Am. Coll. Cardiol.* **58**, 2236–40 (2011).

33. A. M. Kaiser, N. Katkhouda, Laparoscopic management of the perforated viscus., *Semin. Laparosc. Surg.* **9**, 46–53 (2002).

34. D. Rattner, A. Kalloo, ASGE/SAGES Working Group on Natural Orifice Translumenal Endoscopic Surgery, *Surg. Endosc.* **20**, 329–333 (2006).

35. B. a Goff, J. Blake, M. P. Bamberg, T. Hasan, Treatment of ovarian cancer with photodynamic therapy and immunoconjugates in a murine ovarian cancer model., *Br. J. Cancer* **74**, 1194–8 (1996).

36. J. J. McCaughan, Photodynamic therapy: a review, *Drugs Aging* **15**, 49–68 (1999).

37. P. R. Arany, a. Cho, T. D. Hunt, G. Sidhu, K. Shin, E. Hahm, G. X. Huang, J. Weaver, a. C.-H. Chen, B. L. Padwa, M. R. Hamblin, M. H. Barcellos-Hoff, a. B. Kulkarni, D. J. Mooney,

Photoactivation of Endogenous Latent Transforming Growth Factor- 1 Directs Dental Stem Cell Differentiation for Regeneration, *Sci. Transl. Med.* **6**, 238ra69–238ra69 (2014).

43. M. R. Cutkosky, R. D. Howe, in Dexterous Robot Hands, S. Venkataraman, T. Iberall, Eds. Springer-Verlag, 5–31 (1990).

Acknowledgments: We thank the Wyss Institute and the School of Engineering and Applied Sciences. We thank the Animal Research Children's Hospital staff for their overwhelming support and assistance in this project. We thank E. Macomber in Centre for Nanoscale Systems at Harvard for invaluable help with balloon reflective coating. This work was performed in part at the Center for Nanoscale Systems (CNS), a member of the National Nanotechnology Infrastructure Network (NNIN), which is supported by the National Science Foundation under NSF award no. ECS-0335765. CNS is part of Harvard University. We acknowledge M. Smith in Harvard Microbotics Lab, and E. Boggs. We acknowledge A. Abul-Haj from ARA Engineering for expert advice, and for help with light simulations on Zemax software, and R. Abraham from Vention Medical for inner subassemblies. We thank E. Harris, G. Coltof and J. Weaver for assistance with illustrations. We thank Acrolite for fiber sculpting, expertise and repair, J. Weaver for help with energy dispersive electron spectroscopy and R. Bronson for histology consultation. This work was conducted with support from Harvard Catalyst, the Harvard Clinical and Translational Science Center (National Center for Research Resources and the National Center for Advancing Translational Sciences, National Institutes of Health Award UL1 TR001102) and financial contributions from Harvard University and its affiliated academic healthcare centers. The content is solely the responsibility of the authors and does not necessarily represent the official views of Harvard Catalyst, Harvard University and its affiliated academic healthcare centers, or the National Institutes of Health. **Funding:** Translational Research Program grant from Boston Children's Hospital, Wyss Institute for Biologically Inspired Engineering, Harvard School of Engineering and Applied Sciences, E.T.R acknowledges an International Science and Technology Award from Fulbright. This work was also supported by NIH grant GM086433 to J.M.K. and NIH grant R01 HL073647 to P.J.d.N. **Author contributions**: E.T.R, A.F, Y.L, P.P. L.S, N.L., M.J.N.P, I.F., E.F, E.D.O. and S.W were involved in initial brainstorming. E.T.R, A.F, Y.L, P.P. L.S, I.F, A.M.C.B, N.V.V, D.J.M, J.M.K, C.J.W and P.J.d.N further developed the concept. E.T.R, A.F, Y.L, P.P. L.S, E.D.O.C, I.F, A.M.C.B, D.J.M, N.V.V, J.M.K, C.J.W and P.J.d.N designed the experiments. E.T.R, A.F, Y.L, P.P, N.L, and M.J.N.P. performed the in vitro and ex vivo tests. E.T.R, A.F, Y.L, P.P., I.F., A.B, N.V.V, W.W and A.M.C.B. performed the in vivo experiments. E.T.R, A.F, P.P, A.M.C.B., W.W and L.S built and characterized the devices for testing, Y.L. performed the synthesis and Y.L, M.J.P and J.M.K performed the chemical characterization of the adhesive and patches. L.S conducted reflectivity testing with guidance from S.W. A.B. performed the echocardiography and analyzed the images. E.T.R, A.F, Y.L and P.P analyzed the data. E.T.R, A.F, Y.L, P.P., D.J.M, J.M.K., C.J.W and P.J.d.N. wrote the manuscript. All authors provided critical feedback on the manuscript. **Competing interests**: J.M.K. holds equity in and M.J.P is an employee at Gecko Biomedical, a company that has an option to license IP generated and that may benefit financially if the IP is licensed and further validated. The interests of J.M.K were reviewed and are subject to a management plan overseen by his institution in accordance with their conflict of interest policies. Authors have filed patents based on materials described in this manuscript. **Data and materials availability**: All materials or components are commercially available or can be constructed based on the methods.

FIGURE CAPTIONS

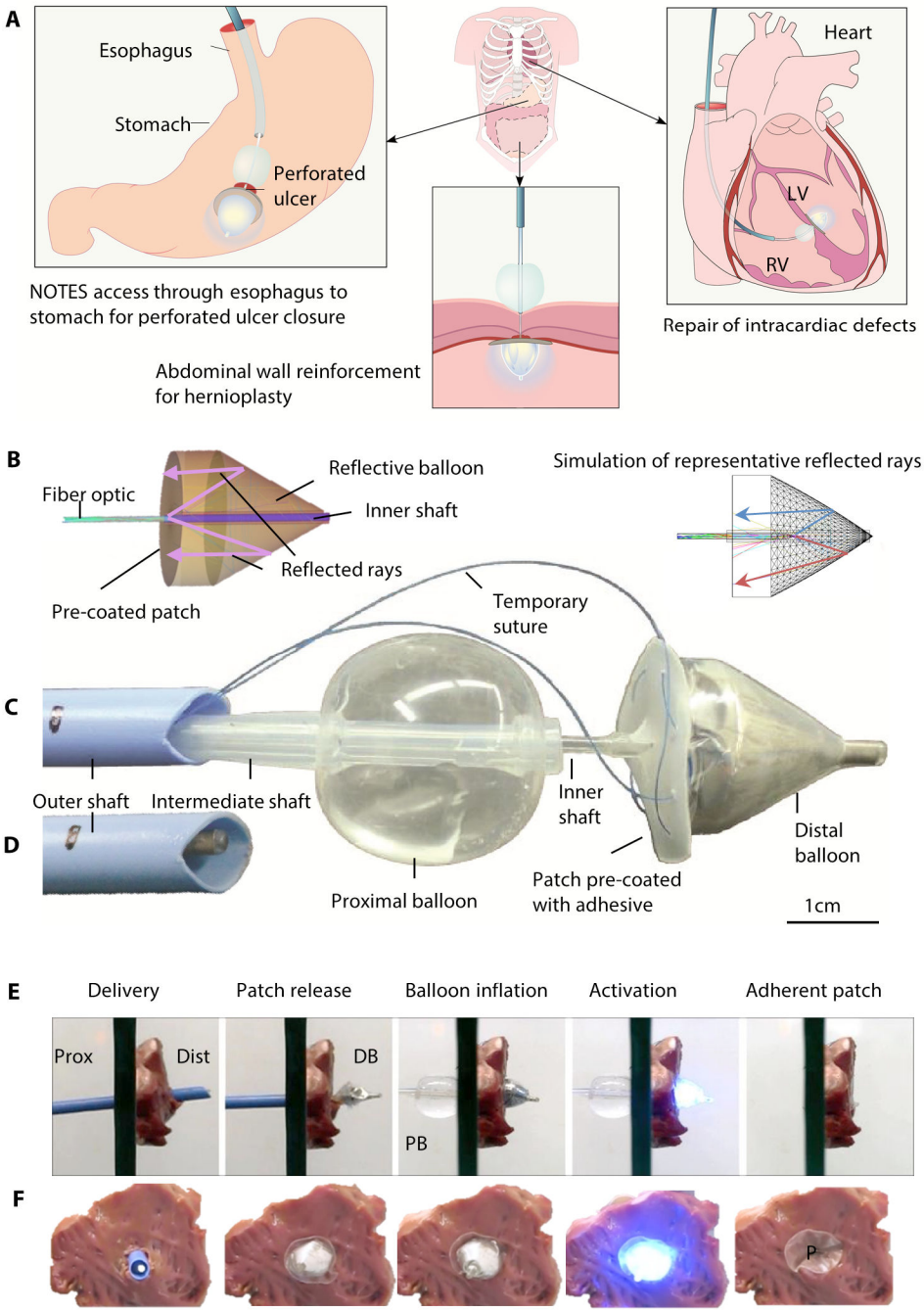

Figure 1: A transcatheter light-reflecting technology that delivers and activates a photocurable adhesive. (**A**) Artistic representation of potential applications for the device, including repair of perforated peptic ulcer, abdominal wall, and intracardiac defects. (**B**) Schematics showing reflection of light rays inside balloon onto a pre-coated patch and a simulation of reflected rays. (**C**) Functional components of the device include the proximal balloon, intermediate shaft, distal balloon with secondary outer balloon and removable sutures for temporary patch/balloon coupling, and the patch with a photocurable adhesive. (**D**) Catheter shaft with functional components loaded and ready for delivery. (**E** and **F**) Procedural steps from

a side (E) and front (F) view on a tissue sample: delivery into cavity, patch release, balloon inflation, adhesive activation, and removal of device after deploying the adherent patch.

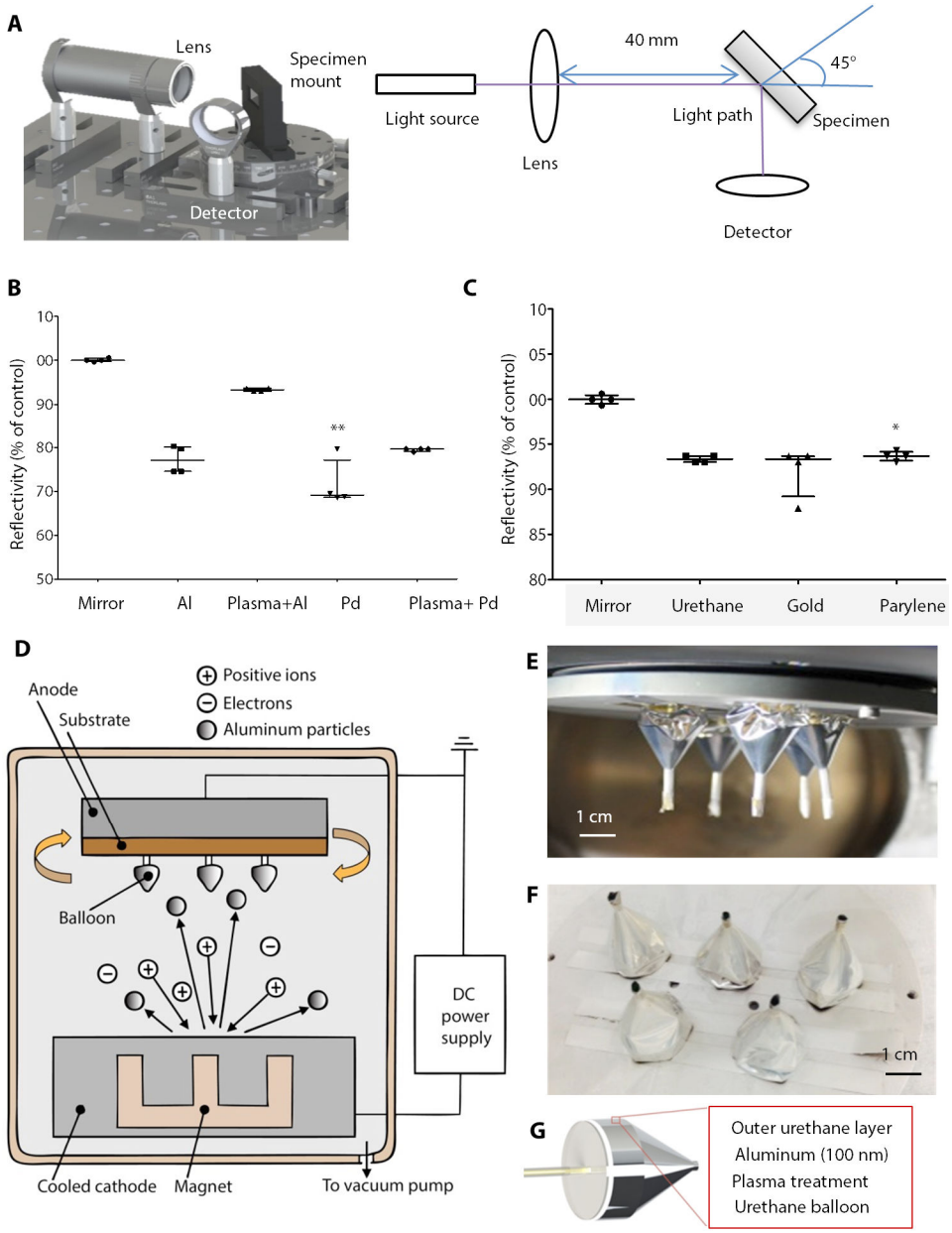

Figure 2: Development and characterization of a light reflective flexible medical balloon. (**A**) Photo and schematic showing coated urethane test specimen mounted at 45 degree angle to a light source with a lens and detector. (**B**) Reflectivity (as a % of a UV enhanced mirror) for urethane samples coated with aluminum (Al) and palladium (Pd) with and without plasma pre-treatment. Data are medians and interquartile ranges ($n = 4$). $^{**}p=0.0022$ compared to mirror. (**C**) Reflectivity (as a % of a UV-enhanced mirror) with outer protective coatings of urethane, parylene, and gold on plasma-treated, aluminum-coated balloons. Data are medians and interquartile ranges ($n = 4$). $^{*}p=0.0197$ compared to mirror. For (B and C), p value was determined with a Kruskall-Wallas test and Dunn's multiple comparison post-hoc test. (**D**) Schematic of sputter coating: DC current was applied to the Al target cathode in argon plasma, Al particles were deposited on the anode, coating the balloons. (**E**) Urethane balloons on the

rotating mount in the sputter chamber during the deposition process. (**F**) Coated balloons. **(G)** Schematic showing the layers of the optimized reflective coated balloons: a protective outer urethane layer, 100 nm of aluminum and plasma-treated urethane balloon.

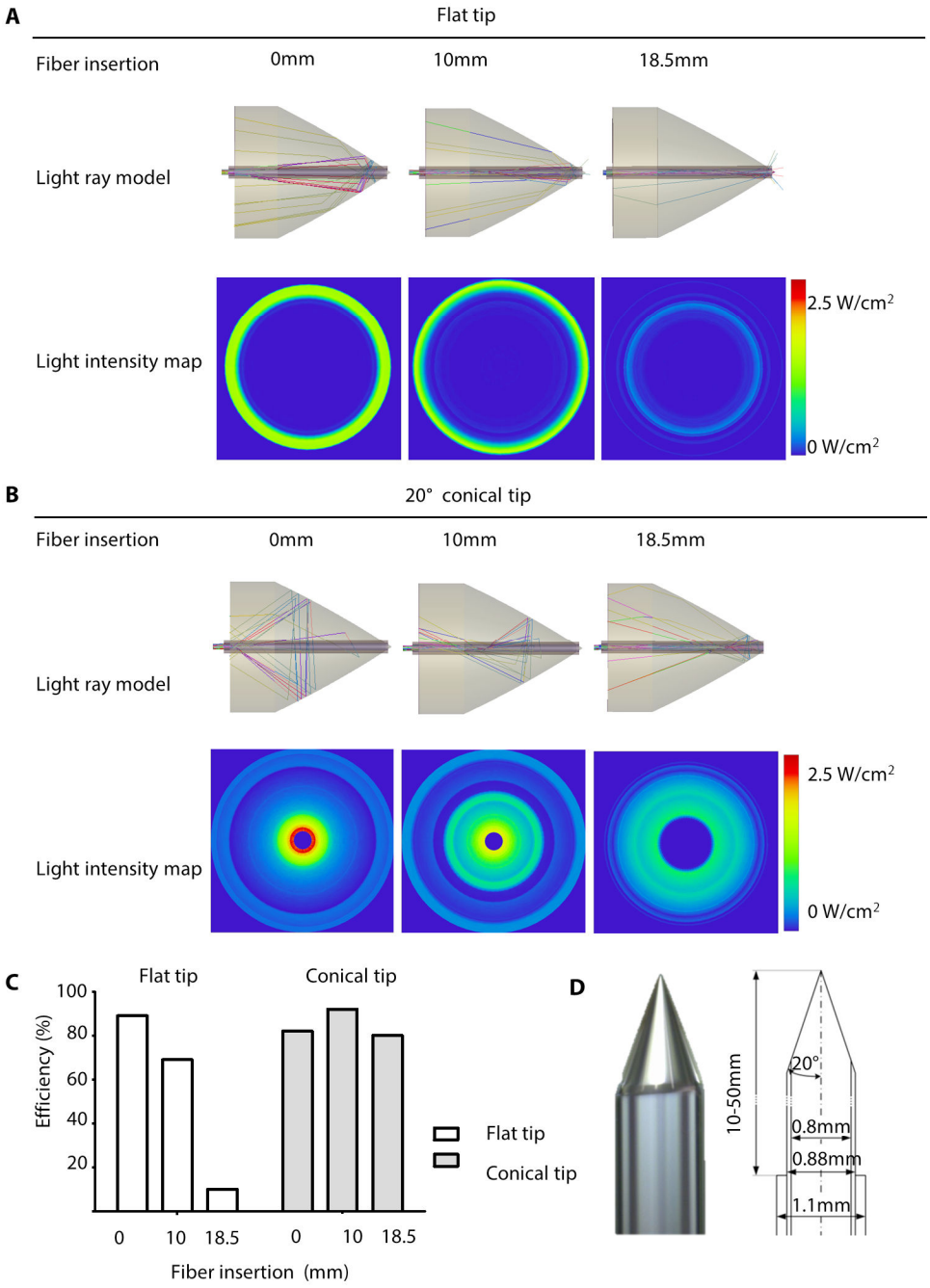

Figure 3: Optimization of a low profile fiber optic for light dispersion. (A and **B)** Light ray model and intensity map on the patch/septum for a flat tip fiber (A) and a conical fiber (20º half-angle) (B) with an insertion distance into the balloon of 0, 10, and 18.5 mm. The images on the top of each panel trace a sample of random rays. The simulations in the bottom of each panel are based on 10^8 rays for a total launched power of 1 W. The efficiency calculations assumed that 100% of the light was available in the fiber before the light was launched into the catheter distances of 0, 10, and 18.5 mm. (**C**) Efficiency (total power at detector divided by input power)

of flat and conical tips. Data are the results of the simulation (*N*=1 for each tip shape) at each catheter insertion distance. **(D)** Sculpted conical fiber optic tip and corresponding dimensions.

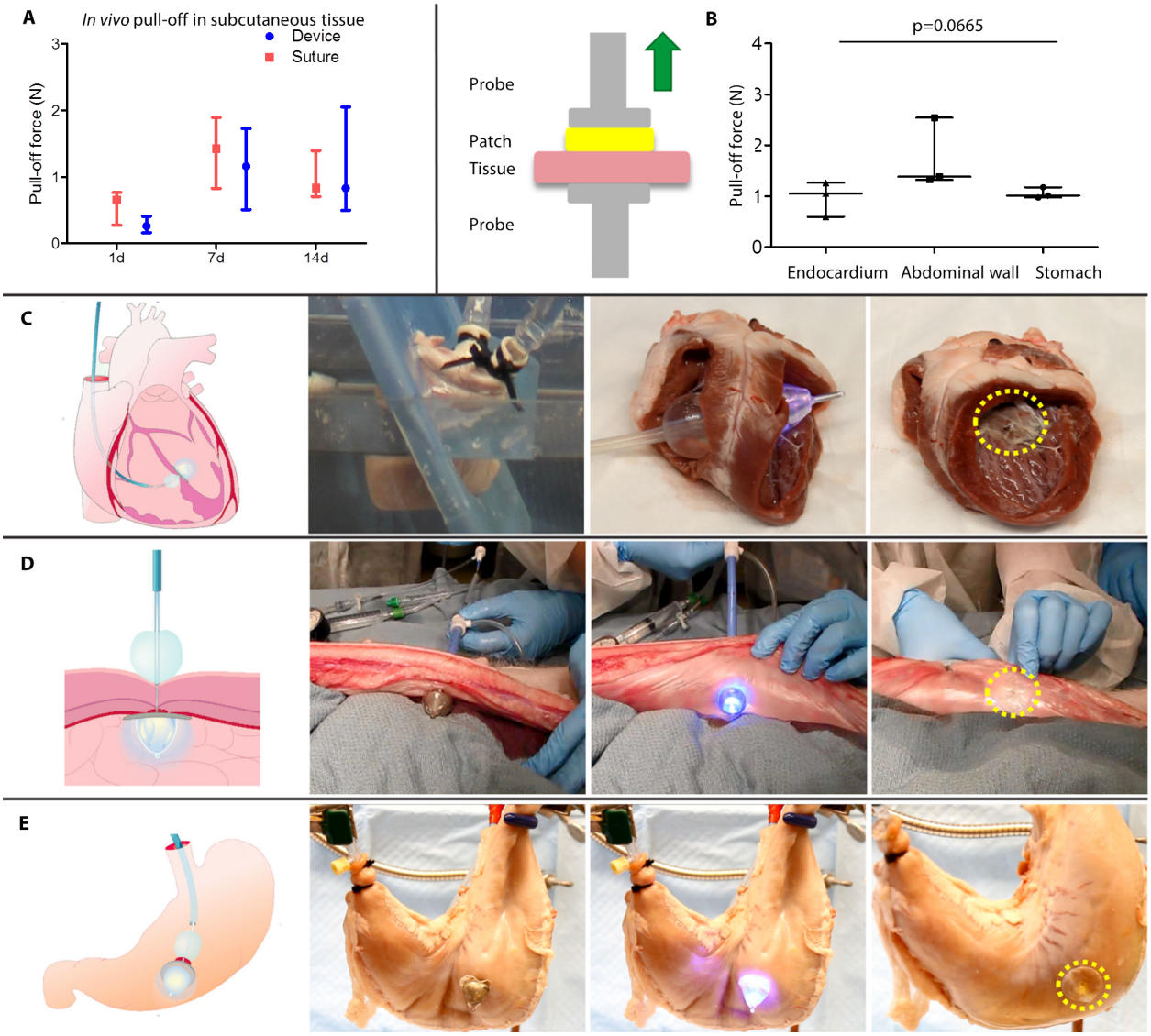

Figure 4: Demonstration of potential clinical applicability *in vivo* and *ex vivo* in porcine heart, abdomen, and stomach. (A) Pull-off force of patch attached by HLAA or suture on abdomen at different time points. Data are medians and interquartile ranges (n=5). P=0.6029 between device and sutures; p=0.0077 for the effect of time; two-way ANOVA. **(B)** Schematic of pull-off testing on a mechanical tester and adhesion pull-off forces for each tissue. Data are represented by a scatterplot with median and interquartile range displayed (*n*=3). *p* value was determined by a Kruskal-Wallis analysis with Dunn's multiple comparison test. **(C)** Proof of concept of ventricular septal defect closure. From left; schematic of device securing patch to porcine left ventricular septal wall, pressurized water-tank set up, the device activating adhesive on bench and adherent patch after device removal and. **(D)** Proof-of-concept of device functionality on porcine abdominal wall. From left; schematic of device fixing patch to back of abdominal wall, delivery, activation and removal of device leaving adhered patch. **(E)** Proof-of-concept of NOTES access for perforated gastric ulcer repair. From left; concept of mouth to esophagus access, device delivery, activation and removal of device with additional adhesive to seal the residual defect, allowing filling of the porcine stomach without leakage.

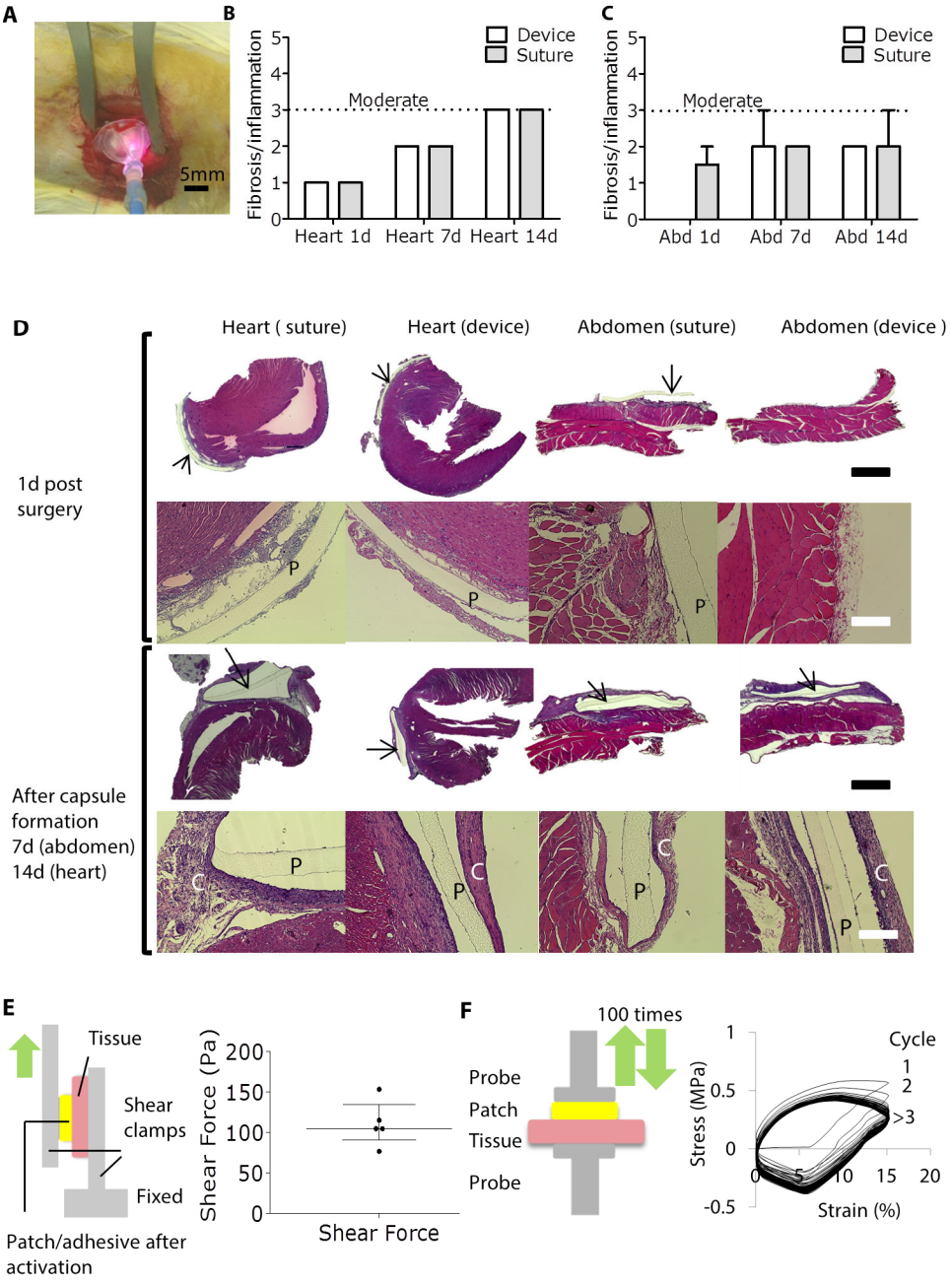

Figure 5: *In vivo* inflammatory response in a rodent model, and shear and cyclical testing. (**A**) Applying the patch to the rat heart using miniaturized device. **(B** and **C)** Degree of fibrosis/inflammation in rat heart and abdomen (abd) samples in response to patches applied by device or with sutures, as determined by a blinded pathologist. Data are means and range (n = 2 per group at each time point). (**D**) Representative histology images 1 day after surgery for heart and abdomen, as well as 1 week post-surgery for abdomen and 2 weeks post-surgery for the heart. PGSU patch denoted by "P" or arrow; capsule, C. Black scale bar, 1 mm; white scale bar, 125 µm. In one case, the patch came off during processing. (**E**) Shear test set-up is shown on the left. Data are in a scatterplot with median and interquartile ranges (n = 5 tissue samples with adhered patches). (**F**) Test set-up and results for cyclical testing of patch/adhesive with tissue (100 compressive cycles).

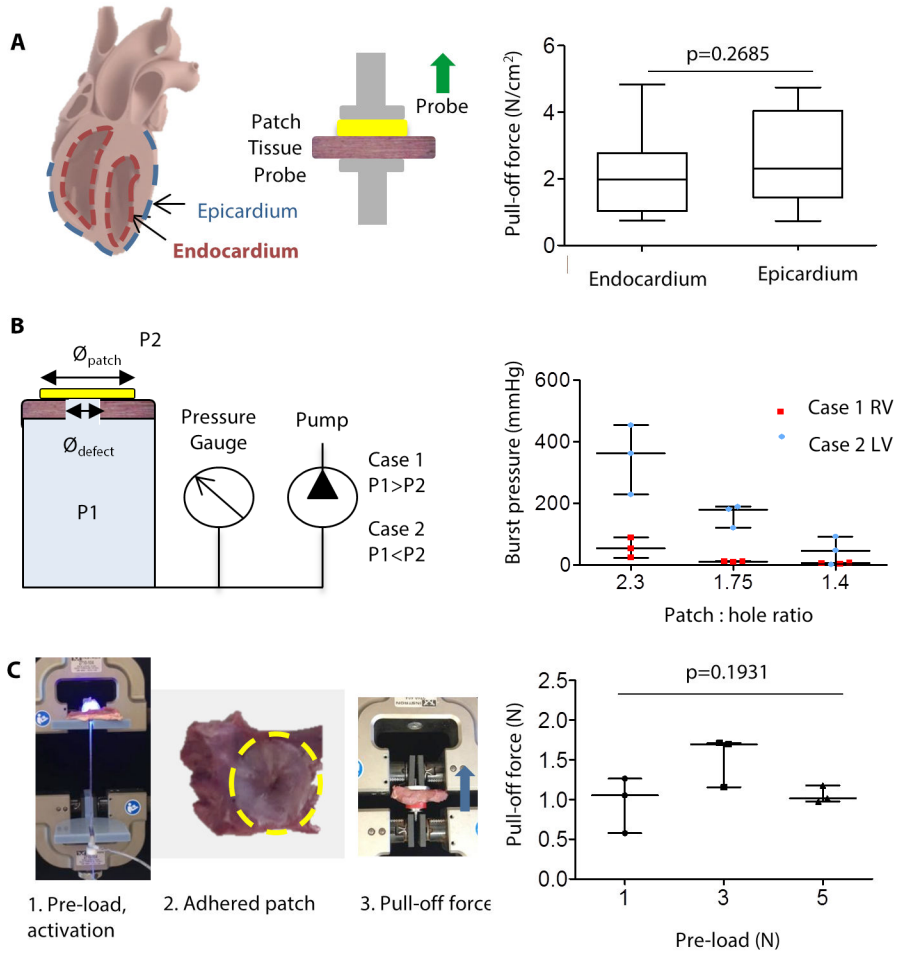

Figure 6: Characterization of device for cardiac-specific applications. (A) Schematic showing endocardial and epicardial surface of the rat heart tissue and apparatus used for pull-off force testing with a mechanical tester and results of pull-off force testing on endocardium and epicardium Data are a box and whiskers plot with median, quartiles and max and min values. *P* value was determined using a two-tailed Mann-Whitney test (*n=17* tissue/patch samples). **(B)** Test set-up for burst pressure testing showing pressurized chamber (at pressure P1) and external pressure P2. R is the ratio between patch and defect diameter. Data are represented by a scatter plot with median and 25% and 75% quartiles (*n*=3-6 tissue samples). **(C)** Test set up for varying pre-load. Data are represented by a scatter plot with median and interquartile range *(n*=3 tissue samples). *P* value was determined by a Kruskal Wallis test with Dunn's multiple comparison post-hoc test.

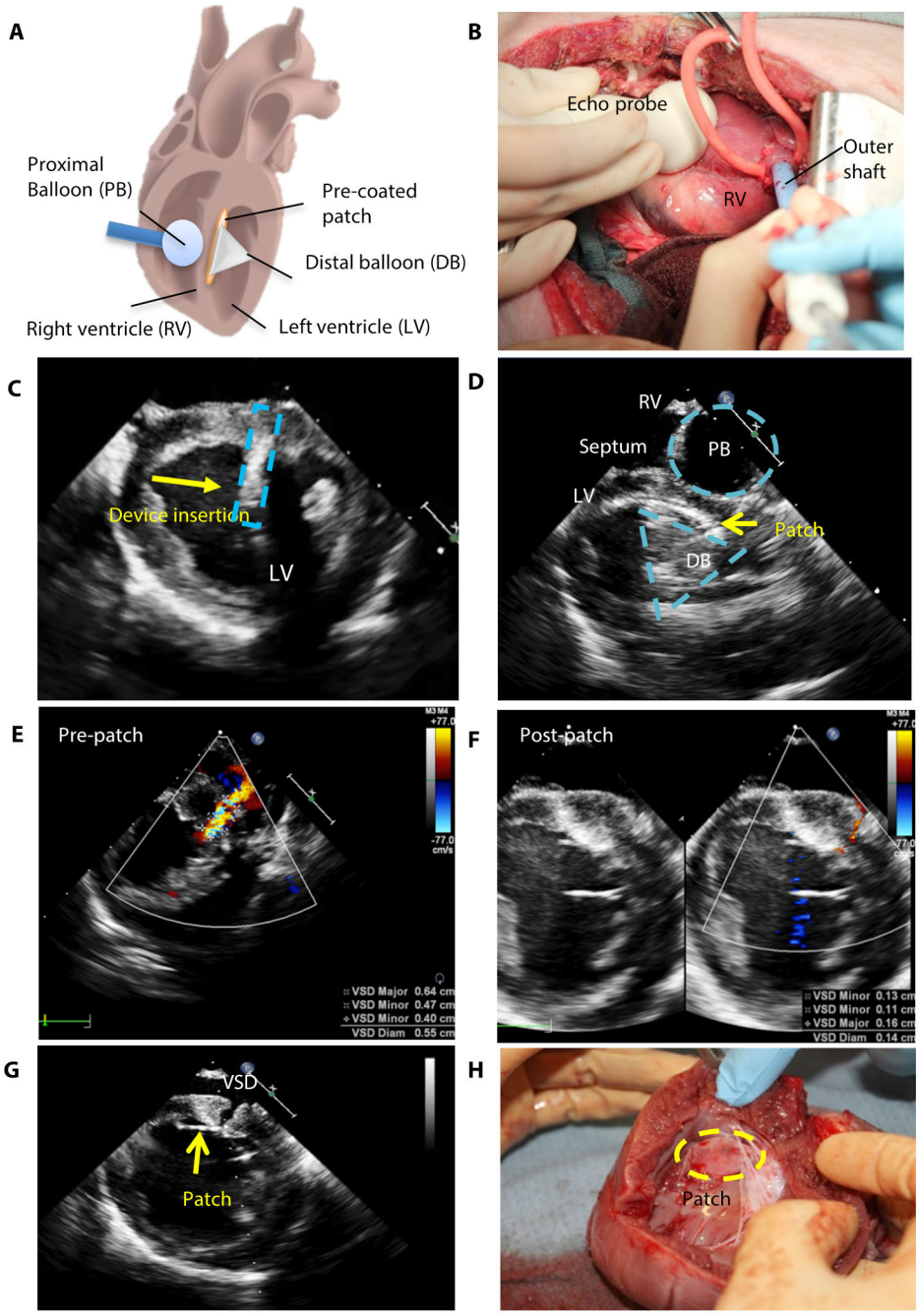

Figure 7: Proof of concept of device reducing porcine ventricular septal defect (VSD) in vivo. (A) A schematic of the device in a cross section of the heart. **(B)** Access for *in vivo* procedure showing anterolateral thoracotomy, position of echo probe and RV access through a purse-string suture, which is used to maintain a seal around the device during the procedure. **(C)** Echocardiograph showing visualization of device insertion into LV (catheter shaft demarcated by dashed blue lines) **(D)** Echocardiograph showing the two inflated balloons (demarcated by blue-dashed lines). **(E)** Echocardiograph with Doppler flow pre-patch implantation showing an average VSD diameter of 5.5 mm. **(F)** Echocardiograph with Doppler flow post-patch implantation showing an average VSD diameter of 1.4 mm. **(G)** Echocardiograph of the patch on the septum VSD. **(H)** Patch adhered on the heart following the procedure.